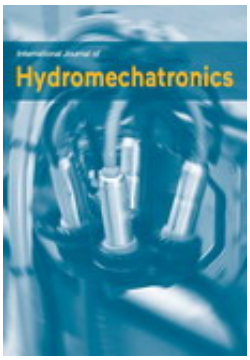

International Journal of Hydromechatronics

ISSN online: 2515-0472 - ISSN print: 2515-0464
https://www.inderscience.com/ijhm

Prescribed performance control for a pneumatic cylinder with strong friction via nonlinear extended state observer

Shaomeng Gu, Ce Yan, Xin Liu, Ling Zhao, Bo Liu

DOI: 10.1504/IJHM.2023.10058748

Article History:

Received:	19 May 2023
Last revised:	11 July 2023
Accepted:	17 July 2023
Published online:	18 October 2023

Prescribed performance control for a pneumatic cylinder with strong friction via nonlinear extended state observer

Shaomeng Gu, Ce Yan and Xin Liu

School of Automation,
Beijing Institute of Technology,
Beijing, China
Email: shaomeng_gu@163.com
Email: yancemc@163.com
Email: liuxin1745@163.com

Ling Zhao*

State Key Laboratory of Fluid Power and Mechatronic Systems,
Zhejiang University,
Hangzhou, China
and
State Key Laboratory of Precision Measuring Technology
and Instruments,
Tianjin University,
Tianjin, China
Email: ling.zhao@tju.edu.cn
*Corresponding author

Bo Liu

Department of Electrical Engineering,
King Fahd University of Petroleum and Minerals,
Dhahran, Saudi Arabia
Email: boliu@kfupm.edu.sa

Abstract: In this paper, a nonlinear extended state observer (NESO)-based prescribed performance control (PPC) method is developed for a pneumatic cylinder with strong friction. For the system model, a pneumatic servo system with strong nonlinearity is established to describe the pneumatic cylinder with strong friction. To improve control accurate under the strong nonlinearity conditions, PPC is design to prescribe its transient and steady-state performances. Moreover, both the NESO convergence and the closed-loop system stability are analysed by utilising Lyapunov approaches. Finally, simulation results and experimental results confirm the effectiveness and robustness.

Keywords: pneumatic servo system; strong nonlinearity; nonlinear extended state observer; NESO; position control; prescribed performance control; PPC.

Reference to this paper should be made as follows: Gu, S., Yan, C., Liu, X., Zhao, L. and Liu, B. (2023) 'Prescribed performance control for a pneumatic cylinder with strong friction via nonlinear extended state observer', *Int. J. Hydromechatronics*, Vol. 6, No. 4, pp.359–379.

Biographical notes: Shaomeng Gu received his BE in Mechanical Design and Manufacturing and Automation from the Guizhou Institute of Technology, Guiyang, China, in 2017. He received his MS in Mechanical Engineering from the Yanshan University, Qinhuangdao, China, in 2020. He is currently pursuing his DEng in Control Engineering with the Beijing Institute of Technology, Beijing, China. His research interests include composite disturbance rejection control, pneumatic systems, and electromechanical systems.

Ce Yan is currently pursuing his PhD with the Beijing Institute of Technology, Beijing, China. His research interests cover cloud control, cloud workflow optimisation scheduling, intelligent transportation, actuator saturation, delta operator, and finite frequency.

Xin Liu is currently pursuing his PhD at the Control Science and Engineering in Beijing Institute of Technology, Beijing, China. His research interests include design and control of pneumatic soft robot.

Ling Zhao received her BS in Automation from the Southwest University, Chongqing, China, in 2007, and PhD in Control Science and Engineering from the Beijing Institute of Technology, Beijing, China, in 2012. She was a teacher in the College of Mechanical Engineering, Yanshan University, Qinhuangdao, China, from 2012 to 2018, where she was promoted to an Associate Professor in 2016. She is currently an Associate Professor with the School of Precision Instruments and Optoelectronics Engineering, Tianjin University, Tianjin, China. She is also with the Taihu Laboratory of Deepsea Technological Science, Wuxi, China. Her research interests include robust control, pneumatic servo control, active disturbance rejection control, and networked control systems.

Bo Liu received his BS in Automatic Control from the North China University of Technology, Beijing, China, in 2005, and PhD in Automatic Control from the Beijing Institute of Technology, Beijing, in 2011. From 2011 to 2015, he was a post-doctoral researcher with the King Fahd University of Petroleum and Minerals (KFUPM), Dhahran, Saudi Arabia, and the King Abdullah University of Science and Technology (KAUST), Thuwal, Saudi Arabia. From 2015 to 2021, he was a research engineer at KFUPM. He is currently a Visiting Assistant Professor with the Electrical Engineering Department, KFUPM. His research interests include control systems, nonlinear filtering, seismic signal processing, and data compression.

1 Introduction

Nowadays, the pneumatic servo system is widely employed in various industries due to its advantages such as safety and light weight (Kato et al., 2018; Stelson, 2018; Kato et al., 2021). However, the strong nonlinearity, which is caused by the air compressibility and friction forces, poses a serious problem in pneumatic servo systems. To address this issue, researchers have proposed several control methods (Wen et al., 2023; Hussaini and Wang, 2022; Ghini and Vacca, 2018). In Qian et al. (2023), a hybrid gaussian mutation particle swarm optimisation method is designed for pneumatic cylinders to improve the tracking accuracy and increase convergence rate. To study the friction characteristics of pneumatic cylinders, a new high-precision friction test platform is developed and widely applied (Qian et al., 2022a). Based on Qian et al. (2022a), the accurate friction model of the pneumatic cylinders is established, and the model is verified by utilising the sliding mode control (SMC) method (Qian et al., 2022b). In Quy-Thinh and Le (2022), the SMC method based on exponential reaching law is proposed to achieve good steady-state performances in systems driven by pneumatic artificial muscles. The abovementioned methods have effectively solved nonlinear problems, however, it is difficult to provide the detailed analysis on transient performances.

Prescribed performance control (PPC) methods can analyse the both transient and steady-state performances for the servo systems (Zhang and Yang, 2017). By introducing an output error conversion function, PPC methods can transform the performance constraint problem on output errors into an unconstrained stabilisation problem (Liang et al., 2023). Moreover, PPC has been successfully applied in various technical systems, including piezo-actuated positioning systems (Nguyen et al., 2018), hypersonic vehicle systems (Xu et al., 2023) and robot joint systems (Karayiannidis et al., 2016). In Hu et al. (2018), adaptive PPC has been designed for the tracking control of a spacecraft to improve both transient and steady-state performances, demonstrating good robustness. In Zhang and Yang (2018), an adaptive fuzzy PPC is proposed for the nonlinear systems with hysteretic actuator faults. Besides PPC, the tracking differentiator (TD) can also improve the transient performances by reducing output overshoot (Han, 2009). In Gu et al. (2023), the TD can also obtain differential signals, which always is used in the design of controller. However, it is hard to deal with nonlinearity in pneumatic cylinders only using PPC and TD (Zhao et al., 2018). For this situation, the extended state observer (ESO) is always employed to solve nonlinear issues, and it has been utilised in various plants, such as pneumatic cylinder systems (Zhao et al., 2018) and double-joint manipulator systems (Zhao et al., 2016). Furthermore, the nonlinear extended state observer (NESO) has also been employed to enhance the robustness of existing control methods, including position control for pneumatic cylinders (Yang et al., 2018) and trajectory tracking control for manipulators systems (Gu et al., 2022). In summary, it is interesting to enhance control abilities of pneumatic servo systems with nonlinearity, which inspires us to investigate this topic.

In this paper, NESO-based PPC is designed for pneumatic cylinder systems with friction to enhance control performances. The main contributions are summarised as below:

1 The NESO is designed to estimate the nonlinearity in real-time, and the parameter ranges of NESO are also obtained by utilising the Lyapunov approach.

2 The NESO-based PPC is proposed to prescribe both transient and steady-state performances, and the proposed method can compensate nonlinearity in real-time.

Finally, simulation results and experimental results demonstrate the viability of the proposed approach.

Notations

In this paper, the superscript T stands for the transpose of the matrix; $|\cdot|$ and $\|\cdot\|$ stands for the absolute value and Euclidean norm, respectively; $\lambda_{\min}\{N\}$ and $\lambda_{\max}\{N\}$ are the minimum and maximum eigenvalue of matrix N, respectively; the function $\text{sign}^r(x) = \text{sign}(x)|x|^r$, where $|x|$ is absolute value, r is a positive number, $\text{sign}(x) = \begin{cases} 1, & x > 0 \\ 0, & x = 0 \\ -1, & x < 0 \end{cases}$ in which $x \in (-\infty, +\infty)$.

2 Problem formulation

2.1 System structure

The pneumatic servo system experimental platform is shown in Figure 1, which is composed of three cylinders in X-axis, Y-axis, and Z-axis. The rodless pneumatic cylinders (SMC, CY1H20-300-Y7BWS) with the stroke of 300 mm in the X-axis and Y-axis are controlled by proportional directional valves (FESTO, MPYE-5-M5-010-B). The vacuum cylinder (SMC, ZCDUKD20-40D) in Z-axis is controlled by a switching valve (SMC, SY3120), and a vacuum chuck is installed at the top of the piston rod. A 12-bit digital-to-analogue card (Advantech, PCL-726) is used to transfer the control command to the proportional valve. Furthermore, a grating displacement sensor (ZK-200) with the resolution of 0.005 mm is connected to the rodless cylinder to measure the displacement. Then, the position signal is transferred to an industrial control computer (Advantech, 610H) by a counting card (Advantech, PCL-833).

2.2 System model

In Figure 2, a schematic diagram for the experimental platform is presented to describe the closed-loop system.

With the help of Figure 2, the dynamical model is established by the Newton's second law:

$$m_p\ddot{y}(t_s) + f_d(t_s) + f_r(t_s) = A_p(p_1(t_s) - p_2(t_s)) = F(t_s) \tag{1}$$

where $\ddot{y}(t_s)$ stands for the piston acceleration, m_p represents the piston mass, A_p stands for the piston area, $f_r(t_s)$ stands for disturbances of the pneumatic cylinder, $p_1(t_s)$ and $p_2(t_s)$ are the pressures, $f_d(t_s) = \iota_0\phi + \iota_1\dot{\phi} + \iota_2\ddot{y}(t_s)$ is the nonlinear friction with ι_0 is the stiffness coefficient, ι_1 represents the damping coefficient, ι_2 stands for the viscous friction coefficient, ϕ means the average deflection (Meng et al., 2013).

Figure 1 The experimental platform with rodless pneumatic cylinder (see online version for colours)

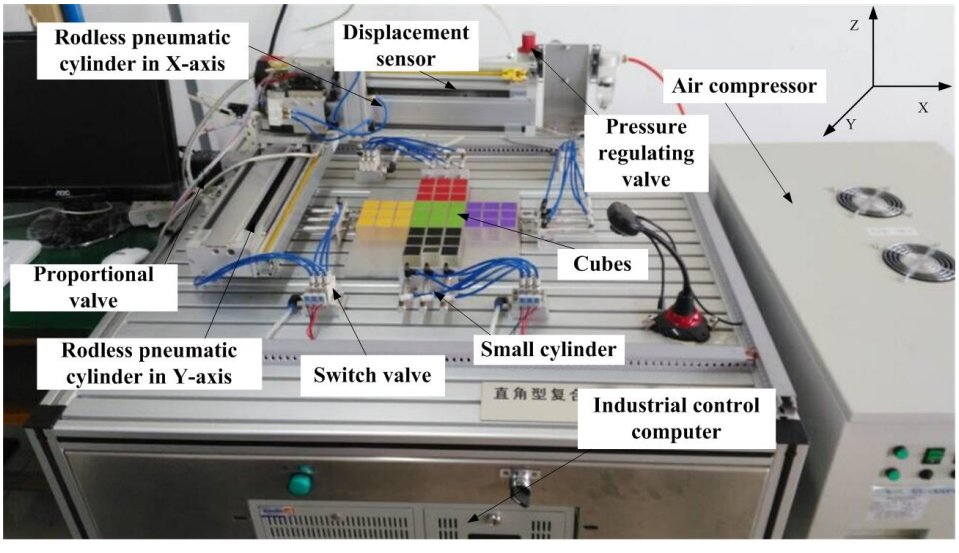

Figure 2 The schematic diagram for the experimental platform (see online version for colours)

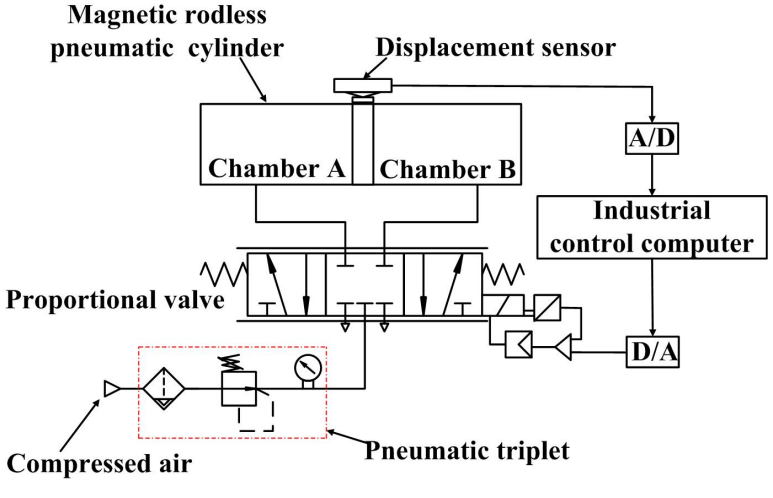

Set $\tilde{\varsigma}_1(t_s) = y(t_s)$, $\tilde{\varsigma}_2(t_s) = \dot{y}(t_s)$ and $F(t_s)/m_p = bu(t_s) + \triangle u(t_s)$, where $u(t_s)$ represents the control input, $\triangle u(t_s)$ stands for the nonlinear part of $u(t_s)$. The dynamical model (1) can be rewritten as:

$$\begin{cases} \dot{\tilde{\varsigma}}_1(t_s) = \tilde{\varsigma}_2(t_s) \\ \dot{\tilde{\varsigma}}_2(t_s) = \triangle u(t_s) - f_d(t_s)/m_p - f_r(t_s)/m_p + bu(t_s). \end{cases} \tag{2}$$

Letting $f(\tilde{\varsigma}_1(t_s), \tilde{\varsigma}_2(t_s)) = \triangle u(t_s) - f_d(t_s)/m_p - f_r(t_s)/m_p$, there exists

$$\begin{cases} \dot{\tilde{\zeta}}_1(t_s) = \tilde{\zeta}_2(t_s) \\ \dot{\tilde{\zeta}}_2(t_s) = f(\tilde{\zeta}_1(t_s), \tilde{\zeta}_2(t_s)) + bu(t_s) \end{cases} \tag{3}$$

where b is the positive constant, $f(\tilde{\zeta}_1(t_s), \tilde{\zeta}_2(t_s))$ represents the strong nonlinearity, which can be simplified to $f(t_s)$.

3 Main results

Considering the strong nonlinearity in the pneumatic servo system (3), the NESO-based PPC method is designed to ensure the response speed and control performances, which includes TD, NESO and prescribed performance controller. To perform the stability analysis, some lemmas are introduced as below.

Lemma 1 (Gu et al., 2023): All eigenvalues of A have negative real parts if and only if for any given positive definite symmetric matrix Q, the Lyapunov equation

$$A^T P + PA = -Q$$

has a unique symmetric solution P and P is positive definite.

Lemma 2 (Zhao et al., 2018): For any positive numbers α, β, γ and positive real numbers m, n satisfying $1/m + 1/n = 1$, the inequality $\alpha\beta \leq \gamma^m \frac{\alpha^m}{m} + \gamma^{-n} \frac{\beta^n}{n}$ holds.

Lemma 3 (Na et al., 2018): If the transformed error $\tilde{\zeta}(t_s)$ is bounded, then the tracking error $\tilde{\vartheta}_1(t_s)$ satisfy with both prescribe transient and steady state performances $t_s \geq 0$, i.e., $-\delta\nu(t_s) < \tilde{\vartheta}_1(t_s) < \delta\nu(t_s)$, where $\nu(t_s) = (\nu_0 - \nu_\infty)e^{-at_s} + \nu_\infty$, $\nu_0 > \nu_\infty > 0$, $\nu_0 > \mid \tilde{\vartheta}_1(0) \mid$, δ and a are two positive constants.

3.1 Tracking differentiator

Overshoot is a negative factor which needs to be suppressed in the pneumatic servo system (3). To address this issue, the TD is employed to arrange the transient process for reducing the overshoot (Zhang et al., 2022). Additionally, the TD can also obtain differential signals, which always is utilised in the controller design (Gu et al., 2023). In this paper, the TD is borrowed from Zhao et al. (2017), which is shown as:

$$\begin{cases} \dot{\tilde{\tau}}_1(t_s) = \tilde{\tau}_2(t_s) \\ \dot{\tilde{\tau}}_2(t_s) = f_h(\tilde{\tau}_1(t_s) - \tilde{\tau}_0(t_s), \tilde{\tau}_2(t_s), r_p, h_p) \end{cases} \tag{4}$$

where r_p and h_p are adjustable positive constants, which can determine speed and smoothness of the transition process, $\tilde{\tau}_0(t_s)$ is the desired signal, $\tilde{\tau}_1(t_s)$ stands for the tracking signal of $\tilde{\tau}_0(t_s)$, $\tilde{\tau}_2(t_s)$ represents the differential signal of $\tilde{\tau}_1(t_s)$. Letting $\iota_p(t_s) = \tilde{\tau}_1(t_s) - \tilde{\tau}_0(t_s)$, the expression of $f_h(\iota_p(t_s), \tilde{\tau}_2(t_s), r_p, h_p)$ is given as follows:

$$f_h(\iota_p(t_s), \tilde{\tau}_2(t_s), r_p, h_p) = \begin{cases} -r_p \text{sign}(a_d(t_s)) & \mid a_d(t_s) \mid > r_p h_p \\ -a_d(t_s)/h_p & \mid a_d(t_s) \mid \leq r_p h_p, \end{cases}$$

where

$$a_d(t_s) = \begin{cases} \tilde{\tau}_2(t_s) + \frac{(\varphi(t_s) - r_p h_p)}{2} \text{sign}(\kappa_p(t_s)) & \mid \kappa_p(t_s) \mid > r_p h_p^2 \\ \tilde{\tau}_2(t_s) + \kappa_p(t_s)/h_p & \mid \kappa_p(t_s) \mid \leq r_p h_p^2. \end{cases}$$

with $\varphi(t_s) = \sqrt{(r_p h_p)^2 + 8 r_p \mid \kappa_p(t_s) \mid}$ and $\kappa_p(t_s) = \iota_p(t_s) + h_p \tilde{\tau}_2(t_s)$.

3.2 Nonlinear extend state observer

It is hard to deal with the nonlinearity in pneumatic servo system (3) only using prescribed performance controller and TD (Zhao et al., 2016). For this situation, the NESO is designed to estimate the nonlinearity $f(t_s)$ in real-time, then the estimated nonlinearity $f(t_s)$ can be compensated in the controller. According to Zhao et al. (2015), the nonlinearity $f(t_s)$ is extended to a new state $\tilde{\varsigma}_3(t_s)$, where $\tilde{\varsigma}_3(t_s)$ is assumed that bounded and differentiable, i.e., $\dot{\tilde{\varsigma}}_3(t_s) = \omega(t_s) \leq \varpi$. Therefore, the extend system can be given as:

$$\begin{cases} \dot{\tilde{\varsigma}}_1(t_s) = \tilde{\varsigma}_2(t_s) \\ \dot{\tilde{\varsigma}}_2(t_s) = \tilde{\varsigma}_3(t_s) + bu(t_s) \\ \dot{\tilde{\varsigma}}_3(t_s) = \omega(t_s). \end{cases} \tag{5}$$

Furthermore, the NESO is designed as:

$$\begin{cases} \dot{\tilde{\pi}}_1(t_s) = \tilde{\pi}_2(t_s) - g_1(f_1(\tilde{\theta}_1(t_s), \tilde{\sigma}) + \tilde{\theta}_1(t_s)) \\ \dot{\tilde{\pi}}_2(t_s) = \tilde{\pi}_3(t_s) - g_2(f_1(\tilde{\theta}_1(t_s), \tilde{\sigma}) + \tilde{\theta}_1(t_s)) + bu(t_s) \\ \dot{\tilde{\pi}}_3(t_s) = -g_3(f_1(\tilde{\theta}_1(t_s), \tilde{\sigma}) + \tilde{\theta}_1(t_s)) \end{cases} \tag{6}$$

where $\tilde{\theta}_1(t_s) = \tilde{\pi}_1(t_s) - \tilde{\varsigma}_1(t_s)$, g_i, $i = 1, 2, 3$, are adjustable parameters, $\tilde{\pi}_i(t_s)$, $i = 1, 2, 3$, are observations of $\tilde{\varsigma}_i(t_s)$, $i = 1, 2, 3$, respectively. For simplicity, $f_1(\tilde{\theta}_1(t_s), \tilde{\sigma}) = \text{sign}^{\tilde{\sigma}}(\tilde{\theta}_1(t_s))$ is indicated by $f_1(\tilde{\theta}_1(t_s))$ with $\tilde{\sigma} \in (0, 1)$.

From the extend system (5) and the NESO (6), an error system is obtained as follows:

$$\begin{cases} \dot{\tilde{\theta}}_1(t_s) = \tilde{\theta}_2(t_s) - g_1\tilde{\theta}_1(t_s) - g_1 f_1(\tilde{\theta}_1(t_s)) \\ \dot{\tilde{\theta}}_2(t_s) = \tilde{\theta}_3(t_s) - g_2\tilde{\theta}_1(t_s) - g_2 f_1(\tilde{\theta}_1(t_s)) \\ \dot{\tilde{\theta}}_3(t_s) = -\omega(t_s) - g_3\tilde{\theta}_1(t_s) - g_3 f_1(\tilde{\theta}_1(t_s)) \end{cases}$$

which can be reorganised as

$$\dot{\tilde{\theta}}(t_s) = A_\theta \tilde{\theta}(t_s) + B_\theta \omega(t_s) - C_\theta f_1(\tilde{\theta}_1(t_s)) \tag{7}$$

where

$$\tilde{\theta}(t_s) = \begin{bmatrix} \tilde{\theta}_1(t_s) \\ \tilde{\theta}_2(t_s) \\ \tilde{\theta}_3(t_s) \end{bmatrix}, A_\theta = \begin{bmatrix} -g_1 & 1 & 0 \\ -g_2 & 0 & 1 \\ -g_3 & 0 & 0 \end{bmatrix}, B_\theta = \begin{bmatrix} 0 \\ 0 \\ -1 \end{bmatrix}, C_\theta = \begin{bmatrix} g_1 \\ g_2 \\ g_3 \end{bmatrix}.$$

Theorem 1: Consider the estimation error system (7), there exist the Hurwitz matrix A_θ and positive definite matrix P_θ satisfying the following matrix inequality

$$A_\theta^T P_\theta + P_\theta A_\theta = -I_3,$$

then the estimation error $\tilde{\theta}(t_s)$ can converge to the region

$$\mathcal{A}_\theta = \left\{ \tilde{\theta}(t_s) | \tilde{\theta}(t_s) \leq \sqrt{\frac{\lambda_{\max}(P_\theta)\varphi_g}{\varrho_\theta \lambda_{\min}(P_\theta)}} \right\},$$

where φ_g is the positive constant, $\varrho_\theta \in (0,1)$ is adjustable.

Proof: The Lyapunov function is selected as:

$$V_\theta(t_s) = \tilde{\theta}^T(t_s) P_\theta \tilde{\theta}(t_s),$$

where P_θ is the positive definite matrix according to Lemma 1. There exists:

$$\begin{aligned}\dot{V}_\theta(t_s) &= \tilde{\theta}^T(t_s)(A_\theta^T P_\theta + P_\theta A_\theta)\tilde{\theta}(t_s) + 2\tilde{\theta}^T(t_s) P_\theta B_\theta \omega(t_s) \\ &\quad - 2\tilde{\theta}^T(t_s) P_\theta C_\theta f_1(\tilde{\theta}_1(t_s)) \\ &\leq -\|\tilde{\theta}(t_s)\|^2 + \epsilon_{g1}\|\tilde{\theta}(t_s)\| + \epsilon_{g2}\|\tilde{\theta}(t_s)\|^{1+\tilde{\sigma}},\end{aligned}$$

where $\epsilon_{g1} = 2\|P_\theta B_\theta\|\varpi$ and $\epsilon_{g2} = 2\|P_\theta C_\theta\|$. According to Lemma 2, we further have

$$\epsilon_{g1}\|\tilde{\theta}(t_s)\| + \epsilon_{g2}\|\tilde{\theta}(t_s)\|^{1+\tilde{\sigma}} \leq \epsilon\|\tilde{\theta}(t_s)\|^2 + \varphi_g$$

where $\epsilon < 1$ and $\varphi_g = \frac{\epsilon^4 \epsilon_{g1}^2}{2} + \frac{1-\tilde{\sigma}}{2}\left(\frac{\epsilon}{1+\tilde{\sigma}}\right)^{\frac{4}{1-\tilde{\sigma}^2}} \epsilon_{g2}^{\frac{2}{1-\tilde{\sigma}}}$. Therefore, we have

$$\dot{V}_\theta(t_s) \leq -\varrho_\theta\|\tilde{\theta}(t_s)\|^2 + \varphi_g \leq -\frac{\varrho_\theta V_\theta(t_s)}{\lambda_{\max}(P_\theta)} + \varphi_g,$$

where $\varrho_\theta = 1 - \epsilon$, which means that

$$V_\theta(t_s) \leq V_\theta(0)\mathrm{e}^{-\frac{\varrho_\theta}{\lambda_{\max}(P_\theta)}t_s} + \frac{\lambda_{\max}(P_\theta)\varphi_g}{\varrho_\theta}(1 - \mathrm{e}^{-\frac{\varrho_\theta}{\lambda_{\max}(P_\theta)}t_s}),$$

and thus

$$\|\tilde{\theta}(t_s)\| \leqslant \sqrt{\frac{V_\theta(0)}{\lambda_{\min}(P_\theta)}}\mathrm{e}^{-\frac{\varrho_\theta}{2\lambda_{\max}(P_\theta)}t_s} + \sqrt{\frac{\lambda_{\max}(P_\theta)\varphi_g}{\varrho_\theta \lambda_{\min}(P_\theta)}}.$$

Finally, the estimation error $\tilde{\theta}(t_s)$ can converge to the region $\mathcal{A}_\theta$. □

3.3 Nonlinear extend state observer-based prescribed performance control

PPC has been widely recognised as an effective technology for analysing both transient and steady-state performances (Zhang and Yang, 2017). By introducing an output error conversion function, PPC can transform the performance constraint problem on output errors into the unconstrained stabilisation problem. Moreover, by introducing the NESO (6), the proposed prescribed performance controller can effectively compensate the nonlinearity in real-time.

According to the pneumatic servo system (3) and the TD (4), the tracking errors are defined as:

$$\begin{cases} \tilde{\vartheta}_1(t_s) = \tilde{\zeta}_1(t_s) - \tilde{\tau}_1(t_s) \\ \tilde{\vartheta}_2(t_s) = \tilde{\zeta}_2(t_s) - \tilde{\tau}_2(t_s). \end{cases}$$

The derivatives of $\vartheta_1(t_s)$ and $\vartheta_2(t_s)$ are calculated as:

$$\begin{cases} \dot{\tilde{\vartheta}}_1(t_s) = \tilde{\vartheta}_2(t_s) \\ \dot{\tilde{\vartheta}}_2(t_s) = \tilde{\zeta}_3(t_s) + bu(t_s) - \dot{\tilde{\tau}}_2(t_s) \\ \qquad\quad = \tilde{\pi}_3(t_s) - \tilde{\theta}_3(t_s) + bu(t_s) - \dot{\tilde{\tau}}_2(t_s). \end{cases} \tag{8}$$

According to Zhang and Yang (2018), set a function as:

$$\tilde{\vartheta}_1(t_s) = S_c(\tilde{\zeta}(t_s))\nu(t_s)$$

where

$$S_c(\tilde{\zeta}(t_s)) = \frac{\delta \mathrm{e}^{\tilde{\zeta}(t_s)} - \delta \mathrm{e}^{-\tilde{\zeta}(t_s)}}{\mathrm{e}^{\tilde{\zeta}(t_s)} + \mathrm{e}^{-\tilde{\zeta}(t_s)}}. \tag{9}$$

Based on (9), there exists:

$$\tilde{\zeta}(t_s) = S_c^{-1}(\lambda(t_s)) = \frac{1}{2}\ln\frac{\lambda(t_s)+\delta}{\delta-\lambda(t_s)}$$

where $\lambda(t_s) = \frac{\tilde{\zeta}_1(t_s)}{\nu(t_s)}$. According to Zhang and Yang (2018), the derivatives of $\tilde{\zeta}(t_s)$ are obtained as:

$$\dot{\tilde{\zeta}}(t_s) = \gamma_c(t_s)\left(\tilde{\vartheta}_2(t_s) - \frac{\tilde{\vartheta}_1(t_s)\dot{\nu}(t_s)}{\nu(t_s)}\right)$$

$$\begin{aligned} \ddot{\tilde{\zeta}}(t_s) = {} & \gamma_c(t_s)\Bigg(bu(t_s) + \tilde{\pi}_3(t_s) - \dot{\tilde{\tau}}_2(t_s) - \frac{\tilde{\vartheta}_2(t_s)\dot{\nu}(t_s)}{\nu(t_s)} - \frac{\tilde{\vartheta}_1(t_s)\ddot{\nu}(t_s)}{\nu(t_s)} - \tilde{\theta}_3(t_s) \\ & + \frac{\tilde{\vartheta}_1(t_s)\dot{\nu}^2(t_s)}{\nu^2(t_s)}\Bigg) + \dot{\gamma}_c(t_s)\left(\tilde{\vartheta}_2(t_s) - \frac{\tilde{\vartheta}_1(t_s)\dot{\nu}(t_s)}{\nu(t_s)}\right) \end{aligned}$$

where $\gamma_c(t_s) = \frac{1}{2\nu(t_s)(\lambda(t_s)+\delta)} - \frac{1}{2\nu(t_s)(\lambda(t_s)-\delta)}$. According to Na et al. (2018), it can be found that $\gamma_c(t_s)$ is bounded. Furthermore, the derivative of $\gamma_c(t_s)$ can be given as:

$$\dot{\gamma}_c(t_s) = -\frac{\tilde{\vartheta}_2(t_s) + \delta\dot{\nu}(t_s)}{2(\tilde{\vartheta}_1(t_s) + \delta\nu(t_s))^2} + \frac{\tilde{\vartheta}_2(t_s) - \delta\dot{\nu}(t_s)}{2(\tilde{\vartheta}_1(t_s) - \delta\nu(t_s))^2}.$$

Setting

$$c_c(t_s) = \tilde{\vartheta}_2(t_s) - \frac{\tilde{\vartheta}_1(t_s)\dot{\nu}(t_s)}{\nu(t_s)},$$

the NESO-based prescribed performance controller is shown as:

$$u(t_s) = \frac{\dot{\tilde{\tau}}_2(t_s) - \tilde{\pi}_3(t_s) + \frac{\tilde{\vartheta}_2(t_s)\dot{\nu}(t_s)}{\nu(t_s)} + \frac{\tilde{\vartheta}_1(t_s)\ddot{\nu}(t_s)}{\nu(t_s)}}{b} - \frac{\frac{\tilde{\vartheta}_1(t_s)\dot{\nu}^2(t_s)}{\nu^2(t_s)} - l\text{sign}(c_c(t_s))}{b} - \frac{\tilde{\zeta}(t_s) + \dot{\gamma}_c(t_s)c_c(t_s)}{b\gamma_c(t_s)} \tag{10}$$

where l is the adjustable parameter.

Theorem 2: Considering the pneumatic servo system (3), there exists the NESO-based prescribed performance controller (10) such that the tracking error system (8) can converge to the adjustable region with the prescribed performances by selecting a large parameter l.

Proof: The Lyapunov function is given as:

$$V_\zeta(t_s) = \frac{1}{2}\tilde{\zeta}^2(t_s) + \frac{1}{2}\dot{\tilde{\zeta}}^2(t_s).$$

Set

$$m(t_s) = \tilde{\pi}_3(t_s) - \tilde{\theta}_3(t_s) + bu(t_s) - \dot{\tilde{\tau}}_2(t_s) + \frac{\tilde{\vartheta}_1(t_s)\dot{\nu}^2(t_s)}{\nu^2(t_s)} - \frac{\tilde{\vartheta}_2(t_s)\dot{\nu}(t_s) + \tilde{\vartheta}_1(t_s)\ddot{\nu}(t_s)}{\nu(t_s)},$$

then we have

$$\begin{aligned}\dot{V}_\zeta(t_s) &= \tilde{\zeta}(t_s)\dot{\tilde{\zeta}}(t_s) + \dot{\tilde{\zeta}}(t_s)\ddot{\tilde{\zeta}}(t_s)\\ &= \gamma_c(t_s)c_c(t_s)[\dot{\gamma}_c(t_s)c_c(t_s) + \gamma_c(t_s)m(t_s) + \tilde{\zeta}(t_s)].\end{aligned}$$

Furthermore, one has that

$$\begin{aligned}\dot{V}_\zeta(t_s) &\le \gamma_c(t_s)c_c(t_s)[-l\gamma_c(t_s)\text{sign}(c_c(t_s)) - \tilde{\theta}_3(t_s)\gamma_c(t_s)]\\ &\le -l\gamma_c^2(t_s)c_c(t_s)\text{sign}(c_c(t_s)) + |\theta_m\gamma_c^2(t_s)c_c(t_s)|\\ &= (-l + |\theta_m|)\gamma_c^2(t_s)c_c(t_s)\text{sign}(c_c(t_s)).\end{aligned}$$

where $\tilde{\theta}_3(t_s)$ is bounded which has been proved in Theorem 1, i.e., $\tilde{\theta}_3(t_s) \le \theta_m$. When $c_c(t_s) \neq 0$ holds, there exists a large parameter l to guarantee $\dot{V}(t_s) \le 0$. When $c_c(t_s) = 0$ holds, there exist $\dot{V}_\zeta(t_s) = 0$ and $\tilde{\vartheta}_2(t_s) = \frac{\tilde{\vartheta}_1(t_s)\dot{\nu}(t_s)}{\nu(t_s)}$. If $\tilde{\vartheta}_2(t_s) = \frac{\tilde{\vartheta}_1(t_s)\dot{\nu}(t_s)}{\nu(t_s)}$ holds, then the following equalities are obtained:

$$\begin{aligned}&\dot{\tilde{\zeta}}(t_s) = 0\\ &\ddot{\tilde{\zeta}}(t_s) = -\tilde{\zeta}(t_s) + \gamma_c(t_s)\tilde{\theta}_3(t_s).\end{aligned}$$

According to $\dot{\tilde{\zeta}}(t_s) = 0$, there exists $\tilde{\zeta}(t_s) = \gamma_c(t_s)\tilde{\theta}_3(t_s)$. It should be pointed that $\gamma_c(t_s)$ and $\tilde{\theta}_3(t_s)$ are bounded which have been proved, therefore, $\tilde{\zeta}(t_s)$ is bounded. For the reason that $\tilde{\zeta}(t_s)$ is bounded, both $\tilde{\vartheta}_1(t_s)$ and $\tilde{\vartheta}_2(t_s)$ are convergent with prescribed performance according to Lemma 3. Therefore, the tracking error system (8) can converge to the adjustable region with prescribed performances. In other words, the proposed method is effective for the pneumatic servo system (3). □

4 Simulations and results

4.1 Simulations with different given desired trajectory signals

In this subsection, numerical simulations of the proposed method have been conducted for the pneumatic servo system (8) to verify the effectiveness. All parameters in numerical simulations have been presented in Table 1, and disturbance $f(t_s)$ is described by the following equation:

$$f(t_s) = \begin{cases} -20\cos(t_s), & t_s \in [0, 8.5] \\ -20\cos(t_s) + 20\sin(t_s), & t_s \in (8.5, 12] \\ -20\cos(t_s) + 20\sin(t_s) - 20\cos(t_s), & t_s \in (12, 20]. \end{cases}$$

Table 1 Simulations parameters

TD	$r_p = 2{,}000$	$h_p = 0.001$		
NESO	$g_1 = 30$	$g_2 = 550$	$g_3 = 2{,}000$	$\sigma = 0.85$
PPC	$\nu_0 = 3$	$\nu_\infty = 0.2$	$a = 0.001$	$l = 50$

Figure 3 Simulation results for the step signal with disturbance $f(t_s)$, (a) position tracking (b) estimation disturbances (c) estimation error (d) tracking error (see online version for colours)

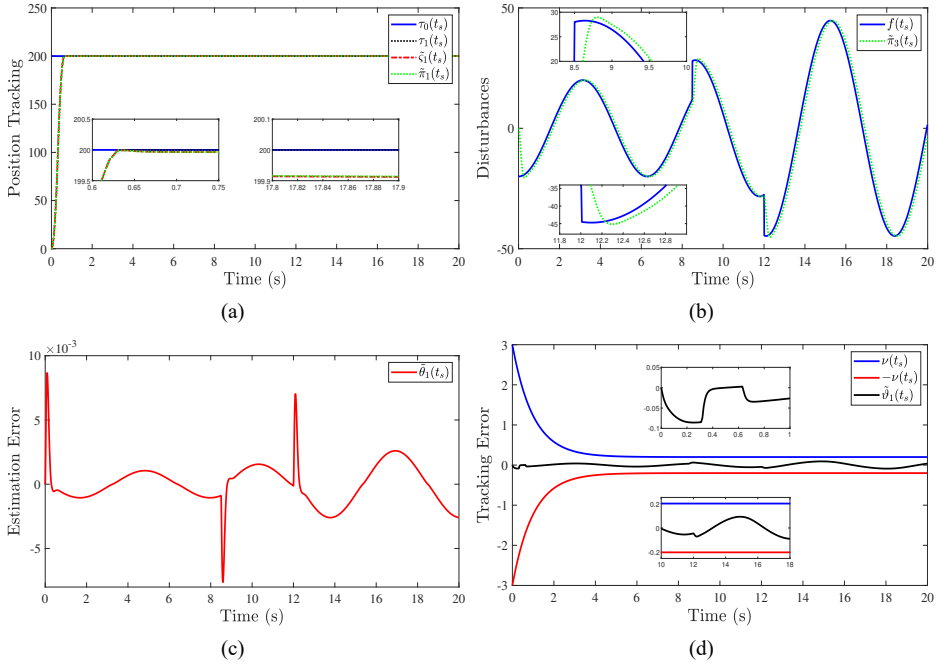

The simulation results on the step signal and the sinusoidal signal are shown in Figures 3–4. It can be seen from Figures 3(a) and 4(a) that the NESO-based PPC method is effective for different given desired trajectory signals. It also can be found from

Figures 3(b)–3(c) and Figure 4(b)–4(c) that for the same disturbances, NESO shows the similar estimation performances under different given desired trajectory signals. Furthermore, in Figures 3(d) and 4(d), when the tracking error $\tilde{\vartheta}_1(t_s)$ is close to the envelop lines, the tracking error $\tilde{\vartheta}_1(t_s)$ is reduced due to constraints of $\nu(t_s)$ and $-\nu(t_s)$.

Figure 4 Simulation results for the sinusoidal signal with disturbance $f(t_s)$, (a) position tracking (b) estimation disturbances (c) estimation error (d) tracking error

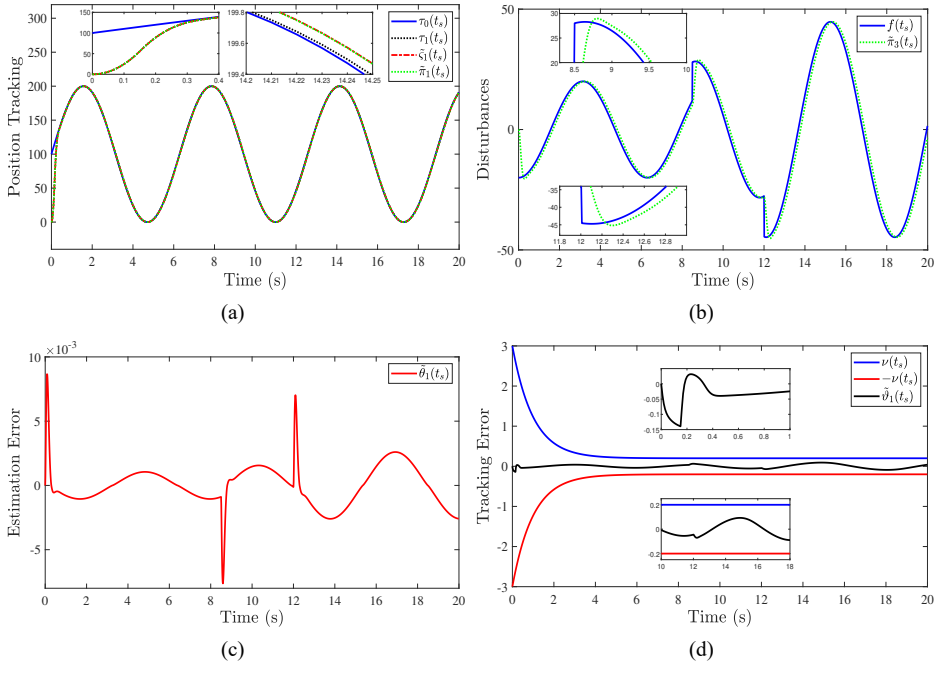

In this simulation, only the given desired trajectory signals are different, and other conditions are completely identical. It should be pointed that the estimation performance of ESO is independent on the given desired trajectory signal, and thus the estimation errors in Figures 3 and 4 are almost no different. The simulation results in Figure 3(c) and 4(c) are consistent with the descriptions in Han (2009), and also corroborate the Theorem 1 in this paper. Moreover, comparing with the tracking errors in Figures 3(d) and 4(d), although the same controller is used in different given desired trajectory signals, it can be found that there are some differences in the transient process. However, because the same controller is applied, there exists the similar steady-state accuracy, which is also consistent with the proposed Theorem 2 in this paper.

4.2 Simulations with different disturbances and controller parameters

In this subsection, the robustness of the proposed method is verified under different load disturbances $f_i(t_s)$ and controller parameters l_i, $i = 1, 2$. The simulation results are divided into two parts.

Figure 5 Simulation results for the sinusoidal signal with disturbance $f_1(t_s)$, (a) position tracking (b) estimation disturbances (c) estimation error (d) tracking error (see online version for colours)

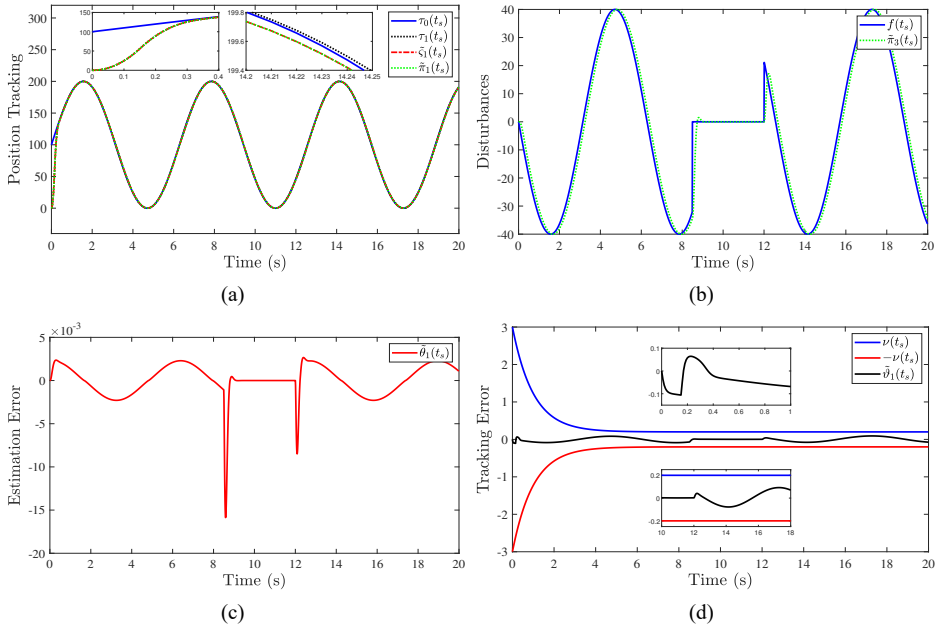

Figure 6 Simulation results for the sinusoidal signal with disturbance $f_1(t_s)$ and $l_1 = 100$, (a) position tracking (b) estimation disturbances (c) estimation error (d) tracking error (see online version for colours)

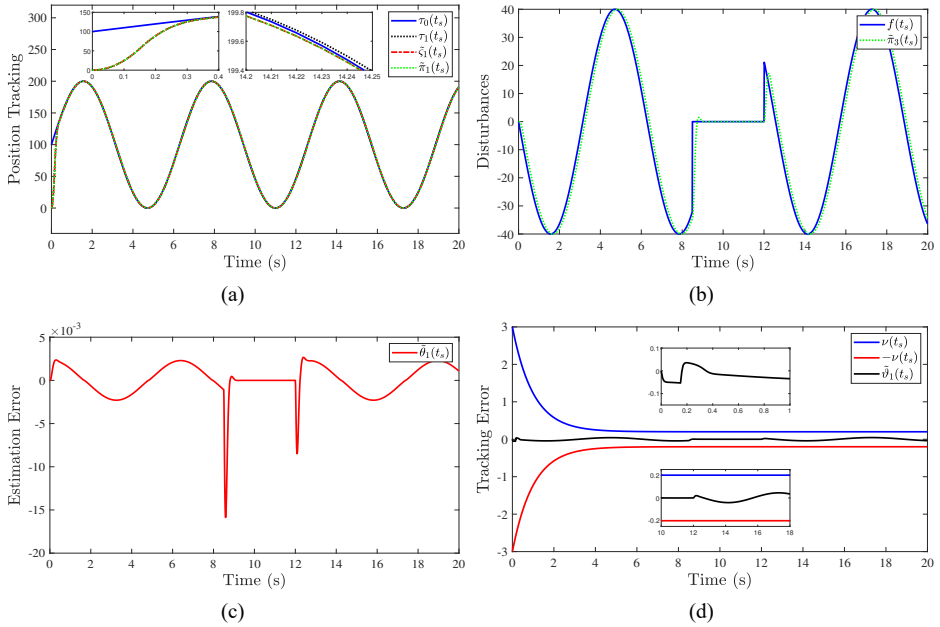

Figure 7 Simulation results for the sinusoidal signal with disturbance $f_2(t_s)$, (a) position tracking (b) estimation disturbances (c) estimation error (d) tracking error (see online version for colours)

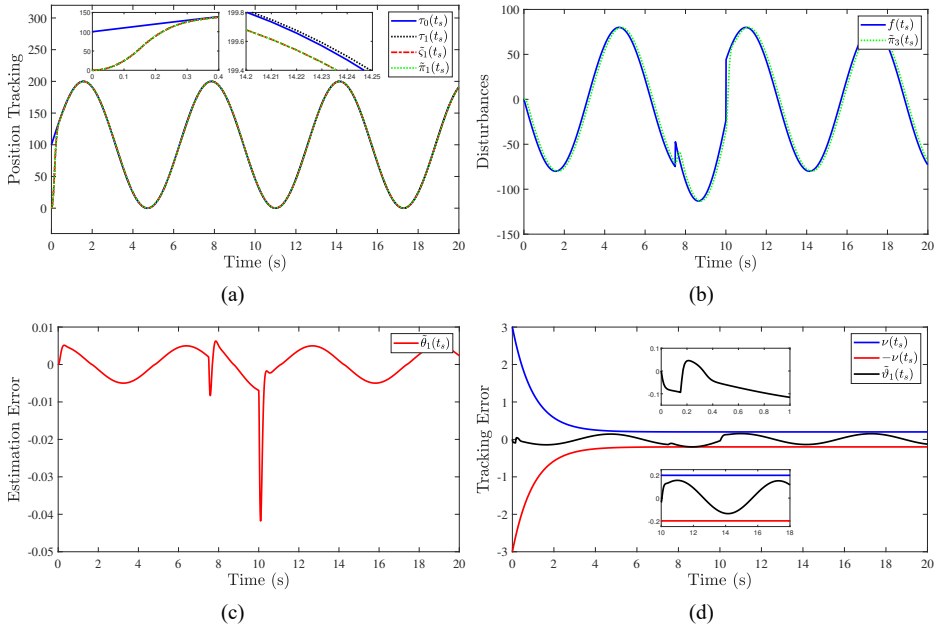

Figure 8 Simulation results for the sinusoidal signal with disturbance $f_2(t_s)$ and $l_2 = 150$, (a) position tracking (d) tracking error (c) estimation error (d) tracking error (see online version for colours)

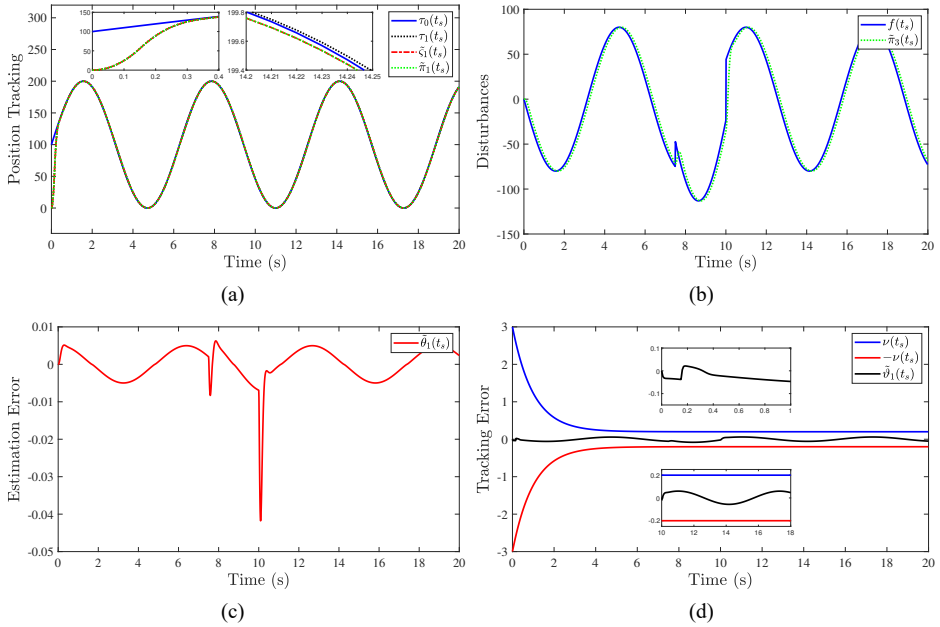

In the first part, the identical simulation parameters are used, and only the different disturbances $f_i(t_s)$, $i = 1, 2$ are introduced into the closed-loop system to verify the robustness of the proposed method, where

$$f_1(t_s) = \begin{cases} -40\sin(t_s), & t_s \in [0, 8.5] \\ -40\sin(t_s) + 40\sin(t_s), & t_s \in (8.5, 12] \\ -40\sin(t_s) + 40\sin(t_s) - 40\sin(t_s), & t_s \in (12, 20], \end{cases}$$

$$f_2(t_s) = \begin{cases} -80\sin(t_s), & t_s \in [0, 7.5] \\ -80\sin(t_s) + 80\cos(t_s), & t_s \in (7.5, 10] \\ -80\sin(t_s) + 80\cos(t_s) - 80\cos(t_s), & t_s \in (10, 20]. \end{cases}$$

The simulation results are depicted in Figures 5 and 7, we can see that the proposed method possesses the robustness for the different disturbances. Moreover, it can be found from Figures 5 and 7 that the disturbances have an impact on the closed-loop system. Specifically, as the disturbance increases, the tracking error of the closed-loop system also increases. However, because the proposed method can estimate and compensate the disturbances, the tracking errors of the closed-loop system can eventually converge to a reasonable region.

In the second part, the different disturbances $f_i(t_s)$ and controller parameters l_i, $i = 1, 2$, are used to verify the robustness of proposed method, where $l_1 = 100$ and $l_2 = 150$. The simulation results are displayed in Figures 6 and 8, we can see that the proposed method with different controller parameters l_i exhibits robustness against diverse disturbances. Moreover, we have further discoveries in the simulation results. Comparing with simulation in Figures 5 and 7, it can be found from Figures 6 and 8 that the controller parameters l_i can influence the tracking error of closed-loop system. Specifically, when the large parameters are chosen, the tracking error of the closed-loop system tends to decrease. The results are consistent with the results of Theorem 2 in the paper.

In summary, according to the above simulations, it can be concluded that the proposed method presented in this paper exhibits robustness and effectiveness. When confronted with significant disturbances, employing larger parameters can enhance the robustness of the proposed method.

5 Experiments and results

In this paper, a single rodless pneumatic cylinder in X-axis is studied, which is shown in Figure 9. The supply pressure is 0.5 MPa and these parameters of component element have been displayed in Table 2.

In the first experiment, the desired signal $\tilde{\tau}_0(t_s)$ is given as a step signal with 200 mm. Main experimental parameters are displayed in Table 3.

In Figure 10(a), $\tilde{\tau}_1(t_s)$ is obtained by using the TD, and $\tilde{\tau}_1(t_s)$ is the tracking signal of $\tilde{\tau}_0(t_s)$. We can see that the output signal $y(t_s)$ and estimation signal $\tilde{\pi}_1(t_s)$ are almost coincident. It can be found from Figure 10(a) that the control precision 0.010 mm and response time 0.40 s are obtained by the proposed control method. Moreover, the control input signal $u(t_s)$ is shown in Figure 10(b), which stand for the voltage signal. In Figure 10(b), it is clear that the input signal $u(t_s)$ keeps at about 5 V after 0.40 s. The tracking error $\tilde{\vartheta}_1(t_s)$ is presented in Figure 10(c). In Figure 10(c), when the

tracking error $\tilde{\vartheta}_1(t_s)$ is close to the envelop lines $\nu(t_s)$ and $-\nu(t_s)$, the tracking error $\tilde{\vartheta}_1(t_s)$ is reduced due to constraints. In Figure 10(d), the estimated nonlinearity $\tilde{\pi}_3(t_s)$ is displayed. We can see that the nonlinearity $\tilde{\pi}_3(t_s)$ reaches steady-state finally, which means that the NESO is effective.

Figure 9 The single pneumatic cylinder (see online version for colours)

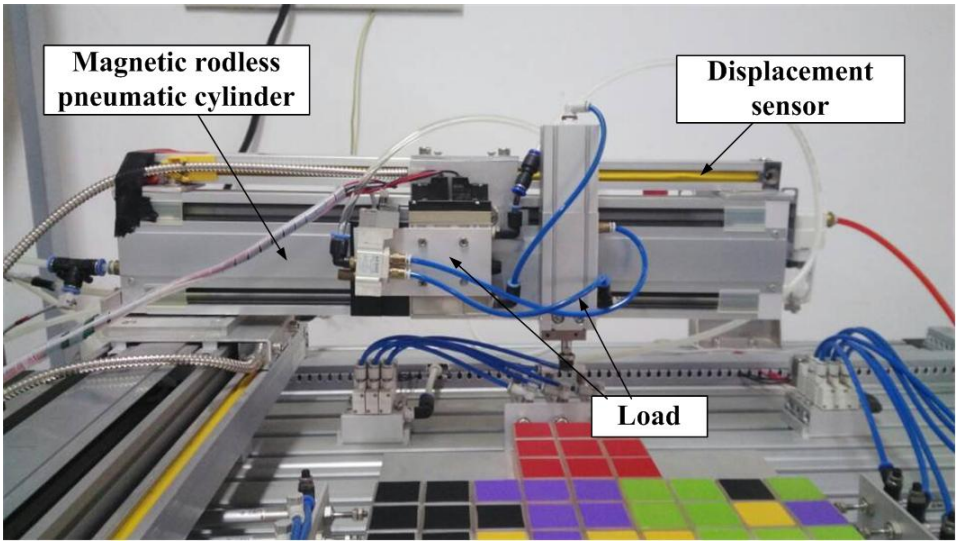

Table 2 The experimental platform parameters

Component element	*Parameter*	*Notes*
Rodless pneumatic cylinders	CY1H20-300-Y7BWS	Working pressure 0–0.7 MPa
Proportional directional valves	MPYE-5-M5-010-B	Dead zone 4.83–5.19 V
Vacuum cylinder	ZCDUKD20-40D	Working pressure 0–0.7 MPa
Switching valve	SY3120	Working pressure 0–0.7 MPa
Grating displacement sensor	ZK-200	Resolution 0.005 mm
Industrial control computer	Advantech, 610H	I5 3470 8G
Digital-to-analogue card	Advantech, PCL-726	12-bit, 6-ch digital I/O
Counting card	Advantech, PCL-833	3-axis quadrature cncoder

Table 3 Main parameters for the step signal

r_p = 8,500	h_p = 0.01	h_0 = 0.02	δ = 1	a = 3.5	ν_0 = 350
b = 1,333	l = 440	g_1 = 100	g_2 = 600	g_3 = 1,000	$\tilde{\tau}_0$ = 200

In the next experiments, the desired signal $\tilde{\tau}_0(t_s)$ is given as a sinusoidal signal. Main experimental parameters are displayed in Table 4.

Experimental results are shown in Figure 12. It can be found that the output signal $y(t_s)$ can track the given desired signal $\tilde{\tau}_0(t_s)$ quickly in Figure 12(a). Moreover, in Figure 12(b), the input signal $u(t_s)$ is shown, and it is obvious that the input signal

$u(t_s)$ periodically changes with fluctuations of position for the pneumatic cylinder. Furthermore, the tracking error $\tilde{\vartheta}_1(t_s)$ is shown in Figure 12(c). In Figure 12(c), the tracking error $\tilde{\vartheta}_1(t_s)$ is reduced due to constraints of $\nu(t_s)$ and $-\nu(t_s)$ when the tracking error $\tilde{\vartheta}_1(t_s)$ is close to the envelop lines. Finally, the estimated nonlinearity $\tilde{\pi}_3(t_s)$ is shown in Figure 12(d). It is clear that the nonlinearity $\tilde{\pi}_3(t_s)$ changes with the trajectory of sinusoidal signal.

Figure 10 Experimental results for the step signal, (a) displacement (b) control input (c) tracking error (d) observed value (see online version for colours)

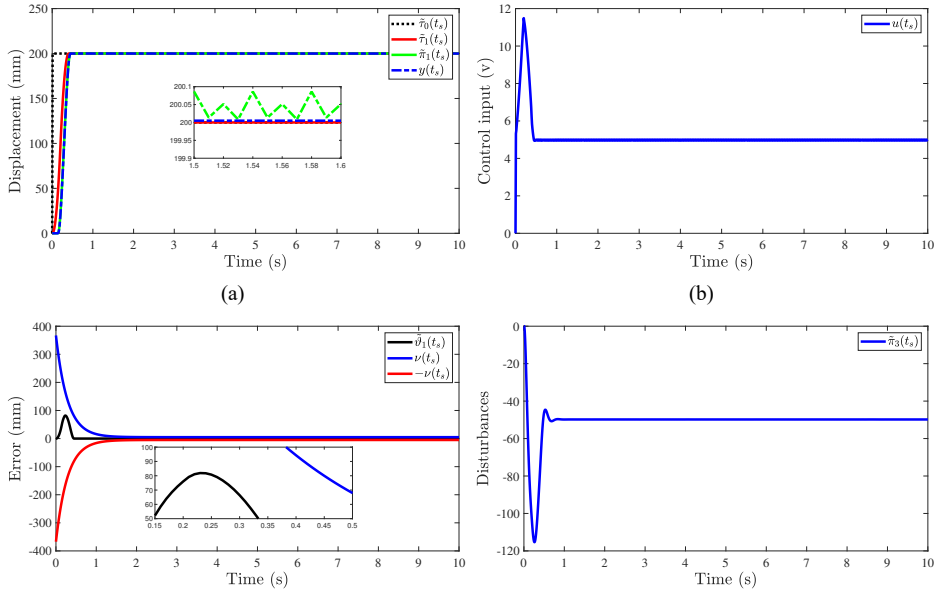

Table 4 Main parameters for the sinusoidal signal

r_p = 7,000	h_p = 0.01	h_0 = 0.02	ν_0 = 350	δ = 1	a = 3.5	b = 950
l = 430	g_1 = 100	g_2 = 600	g_3 = 1,000	$\tilde{\tau}_0$ = 100 sin (0.01πt) + 110		

Table 5 Comparison of experimental results

	Response time	*Steady-state error*
Zhao et al. (2015)	1.0 s	0.050 mm
Zhao et al. (2017)	0.5 s	0.050 mm
This paper	0.4 s	0.010 mm

Comparison experiments are conducted between the proposed method in this paper and the methods presented in Zhao et al. (2015) and Zhao et al. (2017). In comparison experiments, the desired signal $\tau_0(t_s)$ with 200 mm are also used, and the experimental results are shown in Figure 11(a). It can be seen from Figure 11(a) that the proposed method possesses better effect than others. Moreover, results on multi-point positioning are displayed in Figure 11(b), and quantitative results are listed in Table 5.

Figure 11 Experimental results for comparisons, (a) comparing with Zhao et al. (2015) and Zhao et al. (2017) (b) multi-point positioning (see online version for colours)

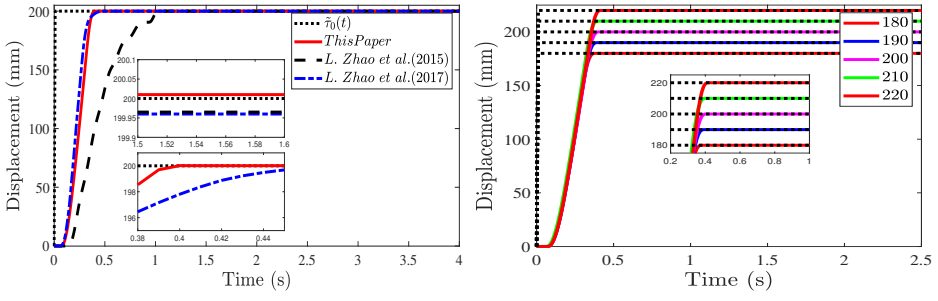

Figure 12 Experimental results for the sinusoidal signal, (a) displacement (b) control input (c) tracking error (d) observed value (see online version for colours)

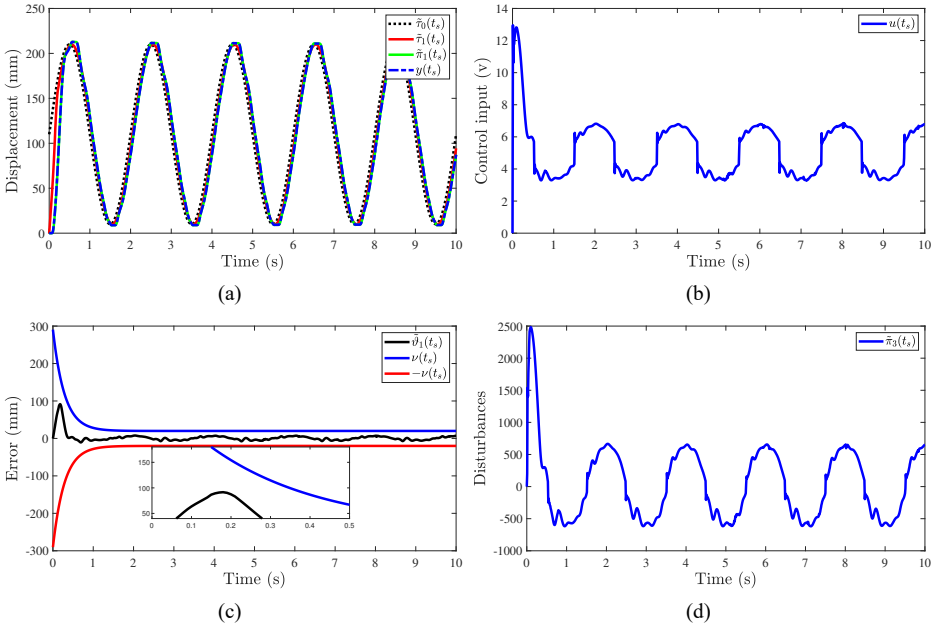

In Figure 11(b), five group experiments with 180 mm–220 mm are conducted, and the similar control performances can be guaranteed for the different signals. According to Table 5 and Figures 10–11, the NESO-based PPC method can enhance the control accuracy and response time.

Remark 1: According to the simulation results and experimental results, we can find that TD only depends on the given signal $\tilde{\tau}_0(t_s)$, thus there exists similar effect in simulations and experiments for arranging the transition process. Compared to experimental results, simulation results possess better tracking performances due to no hardware constraints in simulation. However, both simulation results and experimental results can demonstrate that the proposed method is effective for the closed-loop system.

6 Conclusions

In the paper, NESO-based PPC has been provided to solve the nonlinearity in the pneumatic servo system for improving the transient and steady-state performances of the pneumatic servo system. The proposed method can estimate and compensate the nonlinearity in real-time, moreover, the convergence of the proposed method have been analysed. Finally, the simulation results and experimental results have confirmed the effectiveness and robustness of the NESO-based PPC method. In future work, the finite time PPC will be designed for the nonlinear systems. Moreover, for reducing sampling frequency and calculation time, event-triggered PPC will also be studied.

Acknowledgements

This work was supported by the National Natural Science Foundation of China under Grant 62073238. It was also funded by Open Foundation of the State Key Laboratory of Fluid Power and Mechatronic Systems.

References

Ghini, Y. and Vacca, A. (2018) 'A method to perform prognostics in electro-hydraulic machines: the case of an independent metering controlled hydraulic crane', *International Journal of Hydromechatronics*, Vol. 1, No. 2, pp.197–221.

Gu, S., Zhang, J. and Li, Y. (2023) 'Generalized variable gain ADRC for nonlinear systems and its application to delta parallel manipulators', *IEEE Transactions on Circuits and Systems I: Regular Papers*, Vol. 70, No. 2, pp.921–930.

Gu, S., Zhang, J., Zou, S., Zhao, K. and Ma, Z. (2022) 'Trajectory tracking control for delta parallel manipulators: a variable gain ADRC approach', *IEEE Robotics and Automation Letters*, Vol. 7, No. 3, pp.7747–7754.

Han, J. (2008) *Active Disturbance Rejection Control Technique – The Technique for Estimating and Compensating the Uncertainties*, National Defense Industry Press, Beijing.

Hu, Q., Shao, X. and Guo, L. (2018) 'Adaptive fault-tolerant attitude tracking control of spacecraft with prescribed performance', *IEEE/ASME Transactions on Mechatronics*, Vol. 23, No. 1, pp.331–342.

Hussaini, H. and Wang, C. (2022) 'Battery energy storage system control and integration strategy for the more electric aircraft DC grid application', *International Journal of Hydromechatronics*, Vol. 5, No. 3, pp.275–290.

Karayiannidis, Y., Papageorgiou, D. and Doulgeri, Z. (2016) 'A model-free controller for guaranteed prescribed performance tracking of both robot joint positions and velocities', *IEEE Robotics and Automation Letters*, Vol. 1, No. 1, pp.267–273.

Kato, T., Otsubo, T., Shimazaki, K., Matsuguchi, S., Okamoto, Y. and Yazawa, T. (2018) 'Tool wear estimation method in milling process using air turbine spindle rotation-control system equipped with disturbance force observer', *International Journal of Hydromechatronics*, Vol. 1, No. 4, pp.384–402.

Kato, T., Xu, Y., Tanaka, T., Shotaro, K.S., Okamoto, Y. and Yazawa, T. (2021) 'Force control for ultraprecision hybrid electric-pneumatic vertical-positioning device', *International Journal of Hydromechatronics*, Vol. 4, No. 2, pp.185–201.

Liang, Z., Wang, Z., Zhao, J., Wong, P., Yang, Z. and Ding, Z. (2023) 'Fixed-time prescribed performance path-following control for autonomous vehicle with complete unknown parameters', *IEEE Transactions on Industrial Electronics*, Vol. 70, No. 8, pp.8426–8436.

Meng, D., Tao, G. and Zhu, X. (2013) 'Integrated direct/indirect adaptive robust motion trajectory tracking control of pneumatic cylinders', *International Journal of Control*, Vol. 86, No. 9, pp.1620–1633.

Na, J., Huang, Y., Wu, X., Gao, G., Herrmann, G. and Jiang, J. (2018) 'Active adaptive estimation and control for vehicle suspensions with prescribed performance', *IEEE Transactions on Control Systems Technology*, Vol. 11, No. 6, pp.2063–2077.

Nguyen, M.L., Chen, X. and Yang, F. (2018) 'Discrete-time quasi-sliding-mode control with prescribed performance function and its application to piezo-actuated positioning systems', *IEEE Transactions on Industrial Electronics*, Vol. 65, No. 1, pp.942–950.

Qian, P., Pu, C., Liu, L., Li, X., Zhang, B., Gu, Z. and Meng, D. (2022a) 'Development of a new high-precision friction test platform and experimental study of friction characteristics for pneumatic cylinders', *Measurement Science and Technology*, Vol. 33, No. 6, p.65001.

Qian, P., Pu, C., He, D., Lv, P. and Paez, L.R. (2022b) 'A method to improve the motion trajectory tracking accuracy of pneumatic servo system by exciting longitudinal resonance', *Journal of the Brazilian Society of Mechanical Sciences and Engineering*, Vol. 44, No. 376, pp.1–14.

Qian, P., Luo, H., Liu, L., Lv, P., Pu, C., Meng, D. and Paez, L.R. (2023) 'A hybrid gaussian mutation PSO with search space reduction and its application to intelligent selection of piston seal grooves for homemade pneumatic cylinders', *Engineering Applications of Artificial Intelligence*, Vol. 122, p.106156.

Quy-Thinh, D. and Le, T. (2016) 'Discrete-time sliding mode control on exponential reaching law of a pneumatic artificial muscle actuator', *Journal of Mechanical Engineering*, Vol. 19, No. 1, pp.221–237.

Stelson, A. (2018) 'Academic fluid power research in the USA', *International Journal of Hydromechatronics*, Vol. 1, No. 1, pp.126–152.

Wen, J., Wang, G., Jiaand, J., Li, W., Zhang, C. and Wang, X. (2023) 'Compliance control method for robot joint with variable stiffness', *International Journal of Hydromechatronics*, Vol. 6, No. 16, pp.45–58.

Xu, Z., Sun, C., Hu, X., Liu, Q. and Yao, J. (2023) 'Barrier Lyapunov function-based adaptive output feedback prescribed performance controller for hydraulic systems with uncertainties compensation', *IEEE Transactions on Industrial Electronics*, Vol. 70, No. 12, pp.12500–12510.

Yang, H., Sun, J., Xia, Y. and Zhao, L. (2018) 'Position control for magnetic rodless cylinders with strong static friction', *IEEE Transactions on Industrial Electronics*, Vol. 65, No. 7, pp.5806–5815.

Zhang, J. and Yang, G. (2017) 'Prescribed performance fault-tolerant control of uncertain nonlinear systems with unknown control directions', *IEEE Transactions on Automatic Control*, Vol. 62, No. 12, pp.6529–6535.

Zhang, L. and Yang, G-H. (2018) 'Adaptive fuzzy prescribed performance control of nonlinear systems with hysteretic actuator nonlinearity and faults', *IEEE Transactions on Systems, Man, and Cybernetics: Systems*, Vol. 48, No. 12, pp.2349–2358.

Zhang, J., Cui, C., Gu, S., Wang, T. and Zhao, L. (2022) 'Trajectory tracking control of pneumatic servo system: a variable gain ADRC approach', *IEEE Transactions on Cybernetics*, DOI: 10.1109/TCYB.2022.3174613.

Zhao, L., Yang, Y., Xia, Y. and Liu, Z. (2015) 'Active disturbance rejection position control for a magnetic rodless pneumatic cylinder', *IEEE Transactions on Industrial Electronics*, Vol. 62, No. 9, pp.5838–5846.

Zhao, L., Liu, X. and Wang, T. (2016) 'Trajectory tracking control for double-joint manipulator systems driven by pneumatic artificial muscles based on a nonlinear extended state observer', *Mechanical Systems and Signal Processing* https://doi.org/10.1016/j.ymssp.2018.12.016.

Zhao, L., Xia, Y., Yang, Y. and Liu, Z. (2017) 'Multicontroller positioning strategy for a pneumatic servo system via pressure feedback', *IEEE Transactions on Industrial Electronics*, Vol. 64, No. 6, pp.4800–4809.

Zhao, L., Gu, S., Zhang, J. and Li, S. (2022) 'Finite-time trajectory tracking control for rodless pneumatic cylinder systems with disturbances', *IEEE Transactions on Industrial Electronics*, Vol. 69, No. 4, pp.4137–4147.